# Electric Propulsion With the Sensorless Permanent Magnet Synchronous Motor: Model and Approach

Todd D. Batzel, *Member, IEEE,* and Kwang Y. Lee, *Fellow, IEEE*

***Abstract*—In this paper, a rotor position estimator for the sensorless permanent magnet synchronous motor (PMSM) is developed. The proposed approach exploits the time-scale separation between the electrical and mechanical time constant of the PMSM to formulate a linear observer. The observer produces accurate rotor angle estimates in steady-state and transient, and is attractive for electric propulsion applications due to its independence from mechanical parameters such as load torque, inertia, and friction. The sensorless strategy is well-suited to the nonsaturating slotless PMSM, but the demonstrated robustness of the observer to modeling uncertainties allows for application to slotted construction as well. Experiments are conducted to confirm the effectiveness of the proposed approach.**

***Index Terms*—Brushless machines, electric vehicle, motor control, motor drives, propulsion, sensorless drive, state estimation, torque control, underwater vehicles, variable speed drives.**

## I. Introduction

RECENT advances in power semiconductors, magnetic materials, and energy storage systems have generated considerable interest in the permanent magnet synchronous motor (PMSM) for vehicle propulsion. Electric drives for propulsion can eliminate the need for shafts and gearing while increasing vehicle stealth and power system flexibility. Novel propulsion configurations are pushing the need for the PMSM to operate at the location where torque is required, which in many propulsion systems is a harsh environment due to severe moisture, humidity, vibration, or temperature. In these propulsion systems, conventional rotor angle sensors often cannot be accommodated due to reliability concerns or physical constraints. Thus, there has been an intense interest in the development of the *sensorless* drive, where the PMSM stator itself is used as the rotor position sensor.

Many approaches to sensorless PMSM operation have been reported in literature. The approaches can be categorized as open loop flux estimators, third harmonic voltage-based estimators, back emf waveform detectors, saliency-based position estimators, and model-based observers.

The flux linkage estimation method [1], [2] integrates the difference between phase voltage and stator resistance voltage to estimate the angle of the flux linkage space vector, which is used to produce the appropriate stator current references. This method suffers at low speeds where integrator drift is a serious problem. Furthermore, estimation accuracy is highly sensitive to variations in the stator resistance.

The third harmonic voltage [3], [4] and back emf waveform detection techniques [5], [6] both rely on specific characteristics of the back emf waveform to determine rotor position. Such approaches are applicable to the brushless dc motor but are of little relevance to the PMSM, which ideally has a sinusoidal airgap flux distribution.

For salient rotor PMSM construction, the position-dependent inductance variation can be exploited to obtain a rotor angle estimate [7], [8]. This method is difficult to apply to the widely used surface-mounted PMSM construction whose inductance variation with rotor angle is negligible.

Observers use the actual motor input and output to reconstruct PMSM states such as rotor angle. The pioneering work in [9] implemented a model-based observer to determine rotor angle. This observer was found to be sensitive to mechanical parameters such as load torque, viscous and damping friction, and inertia. In propulsion systems, these parameters are often changing dynamically or are unknown.

Non-linear observers have also been applied to the sensorless PMSM problem in [10], [11], and [12]. In [10], the observer consists of a least squares optimization to fit rotor position and angular velocity to the nonlinear PMSM equations, while [11] constructs the rotor angle and velocity using the relationship between the estimated motor emf and the rotor variables. Both of these approaches implement the PMSM model in the slow time scale by assuming zero inductance. Position estimation is therefore performed in the slow time scale, which may limit the drive bandwidth. Results presented in [11] indicate a large position and speed estimation error during transient due to the limited dynamics of the estimator. In [12], another nonlinear observer is introduced where the acceleration model is included. This approach improves the estimation of position and speed during transient compared to [10] and [11], but unlike those approaches is affected by modeling uncertainty in the mechanical parameters such as viscous friction, inertia, and load torque.

Another approach linearizes the PMSM model using the assumption that angular velocity is constant over the fast sampling interval of the rotor angle observer [13]. Unlike [10] and [11], no assumptions regarding the stator inductance used in the model are made. Since the rotor angle observer views rotor velocity as a time-varying parameter, a separate algorithm is used to estimate rotor speed. This approach results in a linear observer capable of producing accurate rotor angle and velocity estimates in both steady state and transient and exhibiting no dependence on mechanical parameters. This is significant for electric propulsion

Manuscript received November 18, 2003; revised September 22, 2004. This work was supported by the Office of Naval Research under Grant N00014-00-G-0058/007. Paper no. TEC-00338-2003.

T. D. Batzel is with the Department of Electrical Engineering, Penn State Altoona, Altoona, PA 16601 USA (e-mail: tdb120@psu.edu).

K. Y. Lee is with the Department of Electrical Engineering, Pennsylvania State University, University Park, PA 16802 USA (e-mail: kwanglee@psu.edu).

Digital Object Identifier 10.1109/TEC.2005.847948

since the model does not require load torque, inertia, and friction estimates. Although the technique is ideal for the nonsaturating slotless PMSM, it is also applicable to slotted PMSM construction due to its robustness to PMSM modeling uncertainties. In this paper, the angle estimation strategy of [13] is examined and then applied to a prototype vehicle propulsion drive system.

## II. Rotor Position Estimation

In this section, a model-based observer is developed for the estimation of PMSM rotor angle. Conditions for rotor angle observability are examined and closed loop observer pole-placement strategies are set forth.

### A. PMSM Model

The flux linkage model of the nonsalient PMSM in the two-phase stationary reference frame [13] is

$$\begin{bmatrix}\dot{\lambda}_\alpha\\ \dot{\lambda}_\beta\end{bmatrix}=\begin{bmatrix}v_\alpha\\ v_\beta\end{bmatrix}-\tau\left(\begin{bmatrix}\lambda_\alpha\\ \lambda_\beta\end{bmatrix}-\begin{bmatrix}\lambda_{\mathrm{pm}\alpha}\\ \lambda_{\mathrm{pm}\beta}\end{bmatrix}\right);\quad \tau=\frac{R}{\frac{3}{2}L_{\mathrm{av}}}$$
$$\begin{bmatrix}\lambda_{\mathrm{pm}\alpha}\\ \lambda_{\mathrm{pm}\beta}\end{bmatrix}=\sqrt{\frac{3}{2}}\lambda_m\begin{bmatrix}\cos\theta\\ \sin\theta\end{bmatrix}. \tag{1}$$

The terms $\lambda_{\alpha,\beta}$ and $v_{\alpha,\beta}$ represent the flux linkages and voltages corresponding to the two fictitious windings in the stationary reference frame. The symbols $L_{\mathrm{av}}, \lambda_m, R$, and $\theta$ represent the self-inductance, PM flux constant, resistance, and rotor angle, respectively.

To develop the model for a rotor position observer, the vector $[\lambda_{\mathrm{pm}\alpha}\ \lambda_{\mathrm{pm}\beta}]^{\mathrm{T}}$ defined in (1) is considered to be a disturbance state that satisfies a known differential equation. Combining the disturbance state vector with the state variables defined in (1) yields an augmented state vector, $\mathbf{x}$

$$\mathbf{x}=[x_1\quad x_2\quad x_3\quad x_4]^{\mathrm{T}}=[\lambda_\alpha\quad \lambda_\beta\quad \lambda_{\mathrm{pm}\alpha}\quad \lambda_{\mathrm{pm}\beta}]^{\mathrm{T}}. \tag{2}$$

The input vector is the applied phase voltage in the stationary two-phase reference frame

$$\mathbf{u}=[u_1\quad u_2]^{\mathrm{T}}=[v_\alpha\quad v_\beta]^{\mathrm{T}} \tag{3}$$

and the output vector is chosen to be the measurable currents:

$$\mathbf{y}=[y_1\quad \mathrm{y}_2]^{\mathrm{T}}=[i_\alpha\quad i_\beta]^{\mathrm{T}}. \tag{4}$$

The augmented state and output equations [13] are then

$$\dot{\mathbf{x}}=\mathbf{A}_\omega\mathbf{x}+\mathbf{B}\mathbf{u} \tag{5}$$
$$\mathbf{y}=\mathbf{C}\mathbf{x} \tag{6}$$

respectively, where

$$\mathbf{A}_\omega=\begin{bmatrix}-\tau & 0 & \tau & 0\\ 0 & -\tau & 0 & \tau\\ 0 & 0 & 0 & -\omega_e\\ 0 & 0 & \omega_e & 0\end{bmatrix};\quad \mathbf{B}=\begin{bmatrix}1 & 0\\ 0 & 1\\ 0 & 0\\ 0 & 0\end{bmatrix}$$
$$\mathbf{C}=\begin{bmatrix}\tau/R & 0 & -\tau/R & 0\\ 0 & \tau/R & 0 & -\tau/R\end{bmatrix}. \tag{7}$$

The term $\omega_e$ represents the angular velocity of the rotor shaft in electrical radians per second. The subscript $\omega$ associated with the $\mathbf{A}_\omega$ matrix is used to indicate the time varying dependence of that matrix on the rotor angular velocity.

Given the large inertia of the typical PMSM propulsion system and sufficiently fast sampling times, the angular velocity can be assumed to be constant over the system sampling period. With this assumption, the resulting model is a linear time varying system, allowing the use of well-developed linear control methods [14]. It is also stressed that the model given in (5) and (6) does not contain any mechanical variables such as torque, friction, and inertia in the state equations. This is advantageous, since torque and inertia are often unknown and vary during the operation of the typical propulsion system.

### B. Rotor Angle Observer

With angular velocity considered to be a slowly varying parameter, (5) and (6) may be used to construct a full order observer [15]. The observer is used to estimate the state vector $\mathbf{x}$ of (2) from knowledge of the input vector $\mathbf{u}$ and a direct measurement of the output vector $\mathbf{y}$. Note that from the estimation of $x_3$ and $x_4$, the rotor position estimate $\hat{\theta}$ may be determined from

$$\hat{\theta}=\tan^{-1}(\hat{x}_4/\hat{x}_3). \tag{8}$$

Using standard observer design techniques for a linear system [16], the form of the rotor position observer is

$$\dot{\mathbf{e}}=(\mathbf{A}_\omega-\mathbf{G}\mathbf{C})\mathbf{e}. \tag{9}$$

Here $\mathbf{G}$ is the observer gain matrix, $\hat{\mathbf{x}}$ indicates the estimated state vector, and $\mathbf{e}$ is the state estimation error vector

$$\mathbf{e}=\mathbf{x}-\hat{\mathbf{x}}. \tag{10}$$

Convergence of the estimated states toward their actual values is achieved by conventional eigenvalue placement techniques. That is, the eigenvalues of the characteristic equation

$$|\lambda\mathbf{I}-(\mathbf{A}_\omega-\mathbf{G}\mathbf{C})|=0 \tag{11}$$

are chosen to have negative real components so that asymptotic state reconstruction is achieved.

Clearly, observability of the system is a requirement for the estimation of PMSM states. The condition for observability is determined by the rank of the observability matrix [17]

$$\left[\mathbf{C}\quad \mathbf{C}\mathbf{A}_\omega\quad \mathbf{C}\mathbf{A}_\omega^2\quad \mathbf{C}\mathbf{A}_\omega^3\right]^{\mathrm{T}}. \tag{12}$$

The observability matrix of (12) is full rank for nonzero angular velocity so that the system is observable under those conditions. This result supports the well-known drawback of the sensorless PMSM—its inability to estimate rotor angle at zero and low angular velocities [18].

Given the ill-conditioning of the rotor position observer at standstill, special provisions must be made to start the sensorless PMSM and to operate the system at extremely low angular velocity. To accommodate this, the observer gain matrix $\mathbf{G}$ is set to zero at speeds below an experimentally determined low-speed threshold.

### C. Velocity Estimation

It is clear from (7) that rotor velocity is a required parameter for the implementation of the proposed rotor position observer. In addition, angular velocity feedback is required to accurately track the velocity reference in a speed control loop used in some propulsion systems. In the absence of an angular velocity sensor, a suitable strategy must be developed to determine this parameter. Two strategies are now described, and the strengths of each technique are then combined to form an adaptive velocity estimation scheme.

*1) Quasi-Steady State Velocity Estimation:* A quasi steady-state estimate for magnitude of the angular velocity [19] is

$$|\hat{\omega}_e| = \frac{\sqrt{(v_\alpha - \mathrm{Ri}_\alpha)^2 + (v_\beta - \mathrm{Ri}_\beta)^2}}{\sqrt{\frac{3}{2}}\lambda_m}. \tag{13}$$

This result suggests the use of the input and output vectors, $\mathbf{u}$ and $\mathbf{y}$, to estimate the magnitude of the angular velocity. The direction of the angular velocity estimate at sampling interval $k$ is then obtained from

$$\begin{aligned} \hat{\omega}_e &= \mathrm{sgn}(\phi(k) - \phi(k-1))|\hat{\omega}_e| \\ \phi(k) &= \tan^{-1}\left(\frac{\mathrm{Ri}_\alpha(k) - v_\alpha(k)}{v_\beta(k) - \mathrm{Ri}_\beta(k)}\right). \end{aligned} \tag{14}$$

The strength of this method is its ability to determine velocity—even at zero and very low speeds. The weakness is its dependence on PMSM parameters.

*2) Time Derivative of Estimated Rotor Angle:* An alternate method for estimating angular velocity is to use the time derivative of the estimated rotor angle

$$\hat{\omega}_e = d\hat{\theta}/dt. \tag{15}$$

This method obviously requires a stable position observer and that the observer poles have a natural frequency that is high relative to the angular velocity $\omega_e$. These constraints may be enforced at nonzero angular velocity by the proper selection of the system eigenvalues. Subject to these constraints, the estimated angular velocity obtained by (15) approaches the actual value when averaged over a sufficient period of time [19]. The strength of this method is the accurate steady-state speed estimate in the medium to high speed operating range. The drawback, however, is the noise that results from the differentiation process and the incorrect speed estimates that may result during startup. This limits the use of (15) for speed estimation to operation at speeds above a pre-determined low-speed threshold where the angle estimation error has converged toward zero.

*3) Adaptive Velocity Estimation:* The two proposed velocity estimation methods complement each other well. The use of (14) yields good performance at very low speeds, but is subject to parameter uncertainty. The use of (15), however, is essentially independent of the parameter estimation errors so long as the observer poles have a natural frequency much higher than the angular velocity and the velocity is sampled over a sufficient period of time. Thus, the strengths of each method may be combined to form the velocity estimation correction scheme [20], as shown in Fig. 1.

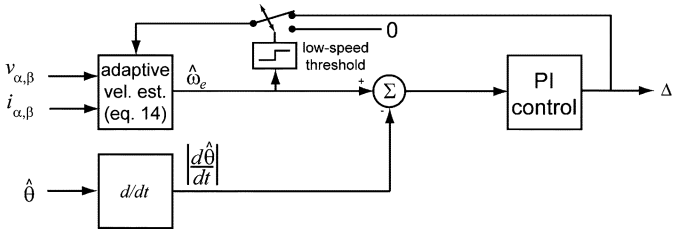


Fig. 1. Adaptive velocity estimation block.

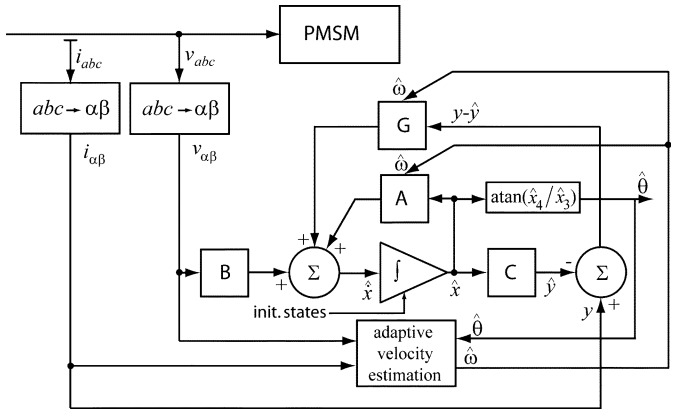


Fig. 2. Block diagram of rotor position estimator.

To use (15) to correct for velocity estimation errors obtained by (14), a modifier $\Delta$ is included to represent the uncertainty in the permanent magnet flux linkage

$$|\hat{\omega}_e| = \frac{\sqrt{(v_\alpha - \mathrm{Ri}_\alpha)^2 + (v_\beta - \mathrm{Ri}_\beta)^2}}{\sqrt{\frac{3}{2}}(\lambda_m + \Delta)}. \tag{16}$$

The adaptation process compares the output of (16) with (15) to generate the velocity estimation error. As long as the magnitude of the speed estimate of (16) is above the low-speed threshold where the position estimate is assumed to be stable, a PI controller operates on the estimation error, adjusting the output $\Delta$ to correct for the parameter uncertainty. The time constant of the PI controller is chosen to be slow in order to remove noise generated by the differentiation of the rotor angle. The overall block diagram of the proposed position observer, including the angular velocity estimation block $(\hat{\omega})$, is shown in Fig. 2.

### D. Pole Placement

It will be later demonstrated that it is advantageous to select the closed loop observer eigenvalues such that their natural frequency is higher than the angular velocity of the PMSM rotor. With this in mind, the observer eigenvalues are scheduled according to the angular speed of the rotor $\omega_e$

$$\begin{aligned} \lambda_1 &= \lambda_3 = |\omega_e|(-k_{\lambda-\mathrm{real}} + jk_{\lambda-\mathrm{imag}}) \\ \lambda_2 &= \lambda_4 = \lambda_1^* = |\omega_e|(-k_{\lambda-\mathrm{real}} - jk_{\lambda-\mathrm{imag}}) \end{aligned} \tag{17}$$

where $k_{\lambda-\mathrm{real}}$ and $k_{\lambda-i\,\mathrm{mag}}$ define the response and damping characteristics of the observer, and $k_{\lambda-\mathrm{real}} > 0$ to enforce negative real eigenvalue locations. In practice, the magnitude of

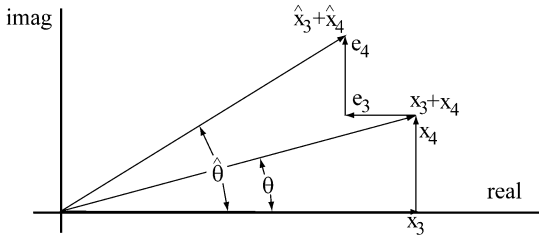


Fig. 3. Effect of state estimation error on angle estimation.

$k_{\lambda-\mathrm{real}}$ is selected such that the angle estimation error $\mathbf{e}$ converges to zero within a satisfactory period of time.

The desired eigenvalue locations given in (17) are enforced through the selection of the observer gain matrix $\mathbf{G}$ in (9). Following the strategy of [16], the solution for the observer gain matrix $\mathbf{G}$ required to place the eigenvalues at the desired locations is obtained [19]:

$$\mathbf{G}=\begin{bmatrix} -R & -\frac{R\lambda_1\lambda_2}{\omega_e\tau} \\ \frac{R\lambda_1\lambda_2}{\omega_e\tau} & -R \\ \frac{R(\lambda_1+\lambda_2)}{\tau} & \frac{R\left(-\lambda_1\lambda_2+\omega_e^2\right)}{\omega_e\tau} \\ -\frac{R\left(-\lambda_1\lambda_2+\omega_e^2\right)}{\omega_e\tau} & \frac{R(\lambda_1+\lambda_2)}{\tau} \end{bmatrix}. \tag{18}$$

Note that the observer gain matrix $\mathbf{G}$ is dependent on the rotor velocity $(\omega_e)$, the desired eigenvalue locations $(\lambda_1,\lambda_2)$, and the PMSM stator winding parameters $(\tau)$. In practice, since velocity is estimated in a sensorless system, the gain matrix $\mathbf{G}$ is calculated using $\hat{\omega}_e$ instead of using $\omega_e$, and the observer gain matrix $\mathbf{G}$ is updated each time a new rotor velocity estimate is generated.

## III. Error Analysis

The error dynamics of the state estimator given by (9) for the full-order observer shows that asymptotic state reconstruction is achieved if the eigenvalues of $\mathbf{A}_\omega-\mathbf{GC}$ have negative reals. In the case where parameter uncertainty is present, the system matrices of the plant and reference model differ, resulting in state reconstruction error. The effects of such parameter uncertainties on the rotor position estimator accuracy are now investigated.

To quantify the effect of parameter uncertainties on rotor angle estimation accuracy, (8) is used with (10) to reveal the relation between the rotor angle estimation error and the error associated with estimated states $\hat{x}_3$ and $\hat{x}_4$

$$\hat{\theta}=\tan^{-1}\left(\frac{x_4-e_4}{x_3-e_3}\right)=\tan^{-1}\left(\frac{\lambda_{\mathrm{pm}\beta}-e_4}{\lambda_{\mathrm{pm}\alpha}-e_3}\right). \tag{19}$$

For the convenience of graphical representation (19) can be expressed as a space phasor

$$Ke^{j\hat{\theta}}=j(\lambda_{\mathrm{pm}\beta}-e_4)+(\lambda_{\mathrm{pm}\alpha}-e_3) \tag{20}$$

where $K$ is the amplitude of the rotating phasor. Fig. 3 demonstrates how state estimation errors $e_3$ and $e_4$ produce a difference between the actual and estimated rotor angles—shown as $\theta$ and $\hat{\theta}$, respectively.

From the state model of (5) and (6), the actual plant behavior can be expressed with respect to the parameter uncertainty and measurement error by

$$\begin{aligned}\dot{\mathbf{x}}&=\tilde{\mathbf{A}}_\omega\mathbf{x}+\Delta\mathbf{A}_\omega\mathbf{x}+\mathbf{B}(\tilde{\mathbf{u}}+\Delta\mathbf{u});\\ \mathbf{y}&=\mathbf{C}\mathbf{x}=\tilde{\mathbf{C}}\mathbf{x}+\Delta\mathbf{C}\mathbf{x}\end{aligned} \tag{21}$$

where $\Delta\mathbf{A}_\omega,\Delta\mathbf{u}$, and $\Delta\mathbf{C}$ represent the uncertainty in the system matrix $\mathbf{A}_\omega$, system input vector $\mathbf{u}$, and the output coupling matrix $\mathbf{C}$ such that

$$\mathbf{A}_\omega=\tilde{\mathbf{A}}_\omega+\Delta\mathbf{A}_\omega;\quad \mathbf{u}=\tilde{\mathbf{u}}+\Delta\mathbf{u};\quad \mathbf{C}=\tilde{\mathbf{C}}+\Delta\mathbf{C}. \tag{22}$$

The values $\tilde{\mathbf{A}}_\omega,\tilde{\mathbf{u}}$, and $\tilde{\mathbf{C}}$ represent the system matrix used by the reference model, the actual input voltage measurement, and the output matrix used by the system model, respectively.

The reference model behaves according to

$$\begin{aligned}\dot{\hat{\mathbf{x}}}&=\tilde{\mathbf{A}}_\omega\hat{\mathbf{x}}+\mathbf{B}\tilde{\mathbf{u}}+\mathbf{G}(\tilde{\mathbf{y}}-\hat{\mathbf{y}})\\ \hat{\mathbf{y}}&=\tilde{\mathbf{C}}\hat{\mathbf{x}}=\tilde{\mathbf{C}}\mathbf{x}+\Delta\mathbf{C}\mathbf{x}\end{aligned} \tag{23}$$

where $\tilde{\mathbf{y}}$ is the measured output current vector. If $\Delta\mathbf{y}$ is the uncertainty in the measured output current

$$\begin{aligned}\mathbf{y}&=\tilde{\mathbf{y}}+\Delta\mathbf{y}\\ \dot{\hat{\mathbf{x}}}&=\tilde{\mathbf{A}}_\omega\hat{\mathbf{x}}+\mathbf{B}\tilde{\mathbf{u}}+\mathbf{G}\tilde{\mathbf{C}}(\mathbf{x}-\hat{\mathbf{x}})+\mathbf{G}\Delta\mathbf{C}\mathbf{x}-\mathbf{G}\Delta\mathbf{y}.\end{aligned} \tag{24}$$

From (9), (21), and (24), the error dynamics are

$$\dot{\mathbf{e}}=(\tilde{\mathbf{A}}_\omega-\mathbf{G}\tilde{\mathbf{C}})\mathbf{e}+\Delta\mathbf{A}_\omega\mathbf{x}+\mathbf{B}\Delta\mathbf{u}-\mathbf{G}\Delta\mathbf{C}\mathbf{x}+\mathbf{G}\Delta\mathbf{y}. \tag{25}$$

In order for the error vector described by (25) to go to zero asymptotically independent of $\mathbf{x}$, $\tilde{\mathbf{A}}_\omega-\mathbf{G}\tilde{\mathbf{C}}$ must be a stable matrix, and the terms $\Delta\mathbf{A}_\omega,\Delta\mathbf{C},\Delta\mathbf{u}$, and $\Delta\mathbf{y}$ must be zero. When these conditions are met, the error dynamics are reduced to the homogeneous equation, and the error approaches zero in steady-state. In practice, the requirement for zero steady-state error is unrealistic. Therefore, the following sections shall analyze the effects of nonzero $\Delta\mathbf{A}_\omega$ and $\Delta\mathbf{C}$ matrices and nonzero $\Delta\mathbf{u}$ and $\Delta\mathbf{y}$ matrices to quantify the effects of modeling uncertainty and signal measurement errors, respectively.

### A. Effects of Modeling Uncertainty and Measurement Errors

*1) Velocity Estimation Error:* For the shaft sensorless PMSM technique previously described, rotor velocity is considered to be a system parameter and therefore must be estimated. The actual rotor angular velocity $\omega_e$ and its estimated value $\hat{\omega}_e$ are related by

$$\omega_e=\hat{\omega}_e+\Delta\omega_e \tag{26}$$

where $\Delta\omega_e$ is the velocity estimation error. Assuming that all parameters except rotor velocity are exactly known, $\Delta\mathbf{y},\Delta\mathbf{C}$, and $\Delta\mathbf{u}$ in (25) are all zero, and the uncertainty in the system matrix due only to velocity estimation error is

$$\Delta\mathbf{A}_{\omega(\omega)}=\begin{bmatrix}0&0&0&0\\0&0&0&0\\0&0&0&-\Delta\omega_e\\0&0&\Delta\omega_e&0\end{bmatrix}. \tag{27}$$

From (25) and (27), the error dynamics with uncertainty in only the angular velocity become

$$\dot{\mathbf{e}} = (\tilde{\mathbf{A}}_{\hat{\omega}} - \mathbf{G}\tilde{\mathbf{C}})\mathbf{e} + \Delta\mathbf{A}_{\omega(\omega)}\mathbf{x}. \tag{28}$$

If the system is stable, the sole contributor to the steady-state error is the forced response of (28), which is then used to determine the angle estimation error from (19). The angle estimation error ($\delta_\omega = \theta - \hat{\theta}$) due to angular velocity uncertainty is found to be [19]

$$\delta_\omega = -\tan^{-1}\left(\frac{\frac{\Delta\omega_e}{\hat{\omega}_e}K_\lambda \cos\phi}{1 - \frac{\Delta\omega_e}{\hat{\omega}_e}K_\lambda \sin\phi}\right)$$
$$K_\lambda = \frac{\omega_e\hat{\omega}_e + \lambda_1\lambda_2}{\left|\sqrt{(\omega_e^2+\lambda_1^2)(\omega_e^2+\lambda_2^2)}\right|};$$
$$\phi = \tan^{-1}\left(\frac{\omega_e^2 - \lambda_1\lambda_2}{(\omega_e(\lambda_1+\lambda_2))}\right). \tag{29}$$

This result implies that for a given operating condition and observer gain $\mathbf{G}$ (determined by $\lambda_1$ and $\lambda_2$), the position estimation accuracy is dependent on the accuracy of the velocity estimate $\Delta\omega_e$. Furthermore, it shows that selecting the system eigenvalues such that $|\lambda_1, \lambda_2| \gg |\omega_e|$ reduces the effects of velocity estimation error by forcing $\phi$ to approach $-\pi/2$, so that $\delta_\omega$ approaches zero.

*2) Effect of Resistance Uncertainty:* In the PMSM, the most temperature sensitive parameter is the stator winding resistance, which varies linearly over the operating temperature of the machine [21]. To study the effect of a balanced resistance uncertainty on angle estimation error, the relation between the actual stator resistance and the nominal value used by the reference model can be represented by

$$R = \tilde{R} + \Delta R \tag{30}$$

where $\tilde{R}$ is the stator resistance value used by the PMSM internal model, $R$ is the actual PMSM stator resistance, and $\Delta R$ represents the modeling error. Assuming that all other parameters are accurately known, the uncertainty in the system matrix due to resistance modeling error is represented by

$$\Delta\mathbf{A}_{\omega(R)} = \begin{bmatrix} -\beta & 0 & \beta & 0 \\ 0 & -\beta & 0 & \beta \\ 0 & 0 & 0 & 0 \\ 0 & 0 & 0 & 0 \end{bmatrix}; \quad \beta = \frac{\Delta R}{L_s} \tag{31}$$

where $L_s = (3/2)L_{\text{av}}$. The error dynamics defined in (25) are

$$\dot{\mathbf{e}} = \dot{\mathbf{x}} - \dot{\hat{\mathbf{x}}} = (\tilde{\mathbf{A}}_\omega - \mathbf{G}\tilde{\mathbf{C}})\mathbf{e} + \Delta\mathbf{A}_{\omega(R)}\mathbf{x}. \tag{32}$$

Following the same procedure as the development of (29), the steady-state solution to (32) reveals that the steady state angle estimation error due to resistance uncertainty is [19]

$$\delta_R = \tan^{-1}\left(\frac{-\frac{\Delta R}{\omega_e}(I_m \sin\xi)}{\sqrt{\frac{3}{2}}\lambda_m + \frac{\Delta R I_m}{\omega_e}\cos\xi}\right) \tag{33}$$

where $\xi$ represents the angle of the stator current with respect to the generated emf and $I_m$ is the peak stator current in the stationary two-phase reference frame. Since most PMSM drives operate with $\xi$ nearly 0, (33) shows that the effect of stator resistance uncertainty is to introduce a steady rotor angle estimation error of $\delta_R$, whose magnitude is proportional to both the resistance uncertainty and current magnitude, and inversely proportional to angular velocity. If the stator current is in phase with the motional emf (i.e., $\xi = 0$), uncertainty in the stator resistance generates no error in the estimated rotor angle. Similarly, in the case of zero stator current, the numerator goes to zero and no angle estimation errors result. This is an easily justifiable result, since angle estimation of an open circuit stator PMSM does not require knowledge of the stator resistance.

*3) Effect of Stator Inductance Uncertainty:* The characteristics of the angle estimation error due to inductance uncertainty are now analyzed by representing the actual stator inductance as

$$L_s = \tilde{L}_s + \Delta L \tag{34}$$

where $L_s, \tilde{L}_s$, and $\Delta L$ are the actual value, the value used by the reference model, and uncertainty of the stator inductance, respectively. Uncertainty in the system matrix due only to inductance modeling error is given by

$$\Delta\mathbf{A}_{\omega(L)} = \begin{bmatrix} R\alpha & 0 & -R\alpha & 0 \\ 0 & R\alpha & 0 & -R\alpha \\ 0 & 0 & 0 & 0 \\ 0 & 0 & 0 & 0 \end{bmatrix};$$
$$\alpha = \frac{\Delta L}{\tilde{L}_s(\tilde{L}_s + \Delta L)}. \tag{35}$$

In addition, any inductance error will result in a nonzero value for $\Delta\mathbf{C}$, which can be represented by

$$\Delta\mathbf{C}_{(L)} = \begin{bmatrix} -\alpha & 0 & \alpha & 0 \\ 0 & -\alpha & 0 & \alpha \end{bmatrix}. \tag{36}$$

Given (35) and (36), the error dynamics for the case of inductance modeling error are

$$\dot{\mathbf{e}} = (\tilde{\mathbf{A}}_\omega - \mathbf{G}\tilde{\mathbf{C}})\mathbf{e} + \Delta\mathbf{A}_{\omega(L)}\mathbf{x} - \mathbf{G}\Delta\mathbf{C}_{(L)}\mathbf{x}. \tag{37}$$

The steady-state solution of (37) is [19]

$$\delta_L = \tan^{-1}\left(\frac{-\Delta L I_m \cos\xi}{\sqrt{3/2}\lambda_m - \Delta L I_m \sin\xi}\right). \tag{38}$$

From this result, balanced inductance modeling error introduces a constant angle estimation error $\delta_L$ whose amplitude is proportional to the magnitude of the inductance uncertainty and the stator current amplitude relative to the PM flux linkage constant $\lambda_m$. Given that saturation leads to a reduction in inductance, (38) can be used to evaluate the potential impact of magnetic saturation on angle estimation performance of a saturable slot-type PMSM.

*4) PM Flux Linkage Uncertainty:* Although PM flux linkage is not included in the PMSM reference model of (5)–(7), it is required to estimate angular velocity (13). Not including the adaptive correction scheme of (16), PM flux linkage uncertainty would generate velocity estimation error. However, with adaptive velocity correction, the effects of PM flux linkage uncertainty are removed.

*5) Effect of Stator Voltage and Current Measurement Errors:* The implementation of the rotor position observer requires the measurement of the stator current and voltage waveforms. The use of these measurements in the rotor position

estimator will result in angle estimation inaccuracy when the sensed quantities contain scaling or offset errors. Scaling, or sensitivity error is the difference in the slope of the actual sensor transfer function and the ideal transfer function. Offset error is any constant value added to the output voltage of the sensor. Assuming zero modeling uncertainty in the presence of current and voltage sensing errors, the error dynamics of (25) are reduced to

$$\dot{\mathbf{e}} = (\tilde{\mathbf{A}}_\omega - \mathbf{G}\tilde{\mathbf{C}})\mathbf{e} + \mathbf{B}\Delta\mathbf{u} + \mathbf{G}\Delta\mathbf{y} \tag{39}$$

where $\Delta\mathbf{u}$ and $\Delta\mathbf{y}$ are the voltage and current measurement errors, respectively. The steady-state solutions to (39) for balanced voltage measurement and current scaling error acting alone have been determined in [19]. The angle estimation error due to voltage sensor scaling errors acting alone ($\Delta\mathbf{y} = 0$) and current sensor scaling errors acting alone ($\Delta\mathbf{u} = 0$) are

$$\begin{aligned}\delta_{v(s)} &= \tan^{-1}\left(-\Delta V \sin\phi \Big/ \left(\omega_e\left(\sqrt{\frac{3}{2}}\lambda_m - \frac{\Delta V}{\omega_e}\cos\phi\right)\right)\right)\\ \delta_{I(s)} &= \tan^{-1}\left(\frac{-\Delta i(L_s\cos\phi - R(\sin\phi/\omega_e))}{\sqrt{3/2}\lambda_m + (R\Delta i/\omega_e)\cos\phi - \Delta i L_s \sin\phi}\right)\end{aligned} \tag{40}$$

respectively. In (40), $\Delta V$ is the magnitude of the balanced voltage scaling error, $\phi$ is defined in (29), and $\Delta i$ represents the magnitude of the balanced current scaling error. This result shows that voltage and current measurement scaling errors result in a constant angle estimation error whose magnitude is proportional to the severity of the scaling error.

In the case of voltage and current sensor offset errors, an angle estimation error with frequency at twice the fundamental electrical frequency is developed whose amplitude is proportional to the magnitude of the measurement offset [19]. Selecting the magnitude of the closed-loop eigenvalue reals to be much greater than the angular velocity helps to reduce the effect of voltage measurement offsets on the rotor position estimation accuracy.

*6) Voltage Phase Shift Measurement Error:* The direct measurement technique to acquire the phase voltage requires the use of a low-pass filter to remove the high switching frequencies injected by the power output stage. The filtering operation results in a measured phase voltage that is phase shifted from the actual quantity. Using $\mathbf{u}$ and $\tilde{\mathbf{u}}$ to represent the actual average and filtered stator voltages

$$\begin{aligned}\mathbf{u} &= \omega_e\lambda_m\begin{bmatrix}-\sin\omega_e t\\ \cos\omega_e t\end{bmatrix};\\ \tilde{\mathbf{u}} &= \omega_e\lambda_m\begin{bmatrix}-\sin(\omega_e t - \psi)\\ \cos(\omega_e t - \psi)\end{bmatrix}\end{aligned} \tag{41}$$

where $\psi$ represents the delay introduced by the low-pass voltage filter. Using (22) to solve for $\Delta\mathbf{u}$, the steady-state solution to (25) reveals that the low-pass filter tends to generate an angle estimation error given by

$$\delta_{v(\text{phase})} \cong \psi \tag{42}$$

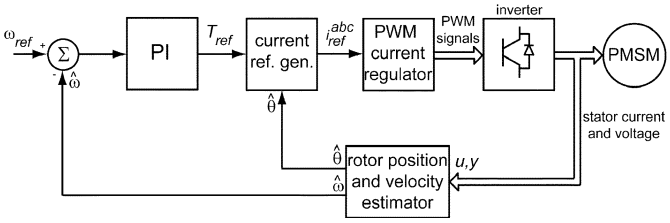


Fig. 4. Block diagram of sensorless PMSM drive system.

for small phase shift $\psi$ [19]. Therefore a phase shift between the actual and measured voltage produces an angle estimation error equal to the angle of the phase shift.

### *B. Eigenvalue Selection Strategy*

The observer poles should be selected according to the system requirements, which are typically rapid response and stable and accurate angle estimation. As the real parts of the eigenvalues become larger negative values, the estimation error converges rapidly. Choosing the eigenvalues too aggressively, however, results in the amplification of system noise and reduced or even unstable performance. Another factor that impacts the eigenvalue selection strategy is the notable outcome of the angle estimation error analysis, which revealed that angle estimation errors due to angular velocity estimation error and signal measurement errors can be reduced by choosing observer eigenvalues to have a high natural frequency relative to the angular velocity of the PMSM.

To address these trade-offs associated with the eigenvalue placement, a general algorithm for observer pole placement was proposed in (17), where the observer poles are placed based on the rotor velocity. If appropriate values for $k_\lambda$ are selected, this eigenvalue placement strategy reduces angle estimation error by satisfying the requirement that the observer eigenvalues have a relatively high natural frequency with respect to the angular velocity. Furthermore, velocity estimation accuracy using the time derivative of the estimated rotor angle is also improved by choosing fast observer eigenvalues [19].

## IV. Controller Design

In the sensorless drive implementation, the rotor angle and velocity estimator supplies the rotor position and velocity feedback necessary for closed-loop torque and velocity control, respectively. The controller shown in Fig. 4 consists of an inner torque controller and outer velocity control loop.

The outer velocity loop consists of a PI controller that operates on the difference between the speed error to produce a torque reference. The torque reference and estimated rotor angle generate balanced three-phase current references, which are enforced by the PWM current regulator.

In the controller, the problematic operating condition around zero speed is managed by setting the observer gain $\mathbf{G}$ to zero when angular velocity falls below a low-speed threshold, which is 7.5 r/s in the experimental system. In this low-speed condition, the estimated rotor angle is produced by integrating the estimated velocity. This mode of operation is adequate for navigating through the zero speed region over a short time period such as during startup or speed reversal. The eigenvalues of the

TABLE I
MOTOR PARAMETERS

| Parameter | Value |
|---|---|
| Inductance $L_{av}$ | 1.22 mH |
| Resistance $R$ | 0.12 Ω |
| PM Flux Linkage $\lambda_m$ | .166 v-s |
| Rated Power | 7.0 HP |
| Poles | 6 |

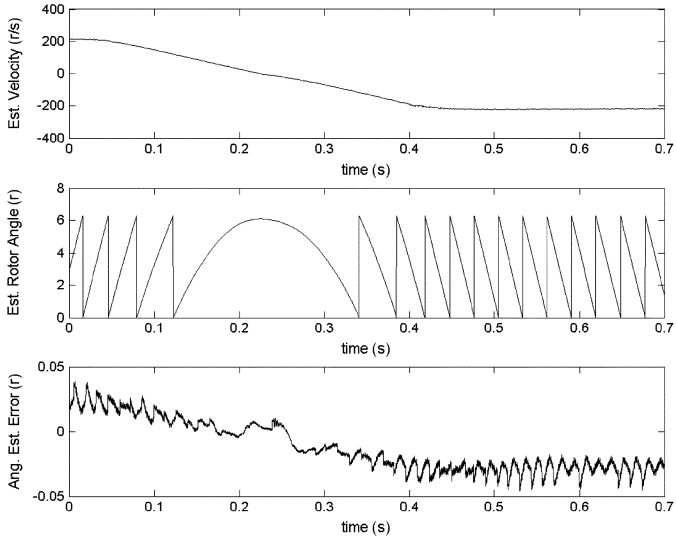


Fig. 5. Angle estimation and speed tracking for fast speed reversal.

position observer are placed according to (17), with $k_{\lambda=\mathrm{real}} = 5$ and $k_{\lambda-i\,\mathrm{mag}} = 2.5$.

The computations required of the controller are carried out by a floating point DSP (Analog Devices Sharc DSP). A fixed-point motor control DSP (Analog Devices (ADMC401) acts as a peripheral to the floating point DSP to implement the current controller, sample the stator voltages and currents, and generate the PWM switching signals.

## V. EXPERIMENTAL RESULTS

To evaluate the performance of the sensorless drive, experiments were performed where the position sensorless controller operates a PMSM of slot-type stator construction in real-time. The performance of the sensorless drive with respect to angle and speed estimation accuracy during acceleration is examined. In addition, the robustness of the estimators to disturbances in the load torque is investigated.

The mechanical arrangement consists of a PMSM, whose shaft is coupled directly to a variable torque load and dynamometer. An encoder attached to the rotor is used only to quantify the accuracy of the estimated angle and velocity. The PMSM parameters are included in Table I.

A significant challenge of the sensorless drive is maintaining control during startup or speed reversal transients. In Fig. 5, a speed reversal is shown to demonstrate the velocity tracking performance for a speed reference with a fast acceleration. In the experiment, the speed is commanded to change from 700 RPM to $-700$ RPM at a rate of 3500 RPM/s. The results indicate excellent rotor position estimation accuracy and velocity tracking

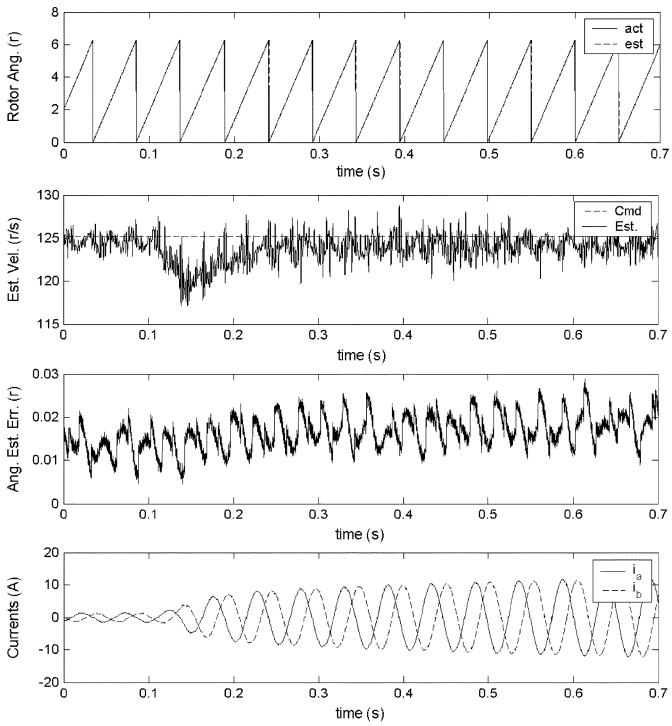


Fig. 6. Load torque change from 0 to 10 ft-lb at .1 sec.

during the transient. Note that the average angle estimation error changes with the frequency of operation. This is due to the filtering of the stator voltage signal as discussed in the error analysis of Section III.

The robustness of the controller to the load torque is demonstrated by applying a sudden load torque of 10 ft-lb to the motor while operating at 400 RPM. As shown in Fig. 6, the load change does not impact the angle estimation accuracy. In addition, the estimated and commanded velocities are nearly identical. This is an attractive feature of the technique, since load torque is often unknown or changing rapidly in propulsion applications.

## VI. CONCLUSION

This paper has presented a sensorless electric drive technique for permanent magnet synchronous motor (PMSM) based propulsion applications. Advantages of the proposed technique include independence from unknown or time-varying mechanical parameters such as load torque, inertia, and friction, and superb performance under transient conditions. Modeling uncertainties arising from data acquisition error and temperature or magnetic effects are considered and the consequences of these uncertainties on angle estimation accuracy are quantified. Experimental results are used to confirm the effectiveness of the developed sensorless drive.

## REFERENCES

[1] R. Wu and G. Slemon, "A permanent magnet motor drive without a shaft sensor," *IEEE Trans. Ind. Appl.*, vol. 27, no. 5, pp. 1005–1011, Sep./Oct. 1991.

[2] A. Consoli, S. Musumeci, A. Raciti, and A. Testa, "Sensorless vector and speed control of brushless motor drives," *IEEE Trans. Ind. Electron.*, vol. 41, no. 1, pp. 91–96, Feb. 1994.

[3] J. Moreira, "Indirect sensing for rotor flux position of permanent magnet AC motors over a wide speed range," *IEEE Trans. Ind. Appl.*, vol. 32, no. 6, pp. 1394–1401, Nov./Dec. 1996.

[4] H. J. Gutt, V. Bosch, and D. Reismayr, "Sensorless direct control of brushless inverter fed permanent magnet excited AC motor drive system," in *Proc. 30th Annu. IEEE Power Electronics Specialists Conf.*, 1999, pp. 838–841.
[5] S. Ogasawara, K. Suzuki, and H. Akagi, "A sensorless brushless DC motor system," *Elec. Eng. Jpn.*, vol. 12, no. 5, pp. 109–117, 1992.
[6] R. C. Beccera, T. M. Jahns, and M. Ehsani, "Four-quadrant sensorless brushless ECM drive," in *Proc. IEEE Appl. Power Electronics Conf. Expo.*, 1991, pp. 202–209.
[7] A. Kulkarni and M. Ehsani, "A novel position sensor elimination technique for the interior permanent magnet synchronous motor drive," *IEEE Trans. Ind. Appl.*, vol. 28, no. 1, pp. 144–150, Jan./Feb. 1992.
[8] V. Petrovic and A. M. Stankovic, "Saliency-based position estimation in PM synchronous motors," in *Proc. Conf. Rec. 36th Annu. Industry Applications Conf.*, 2001, pp. 801–806.
[9] L. Jones and J. Lang, "A state observer for the permanent magnet synchronous motor," *IEEE Trans. Ind. Electron.*, vol. 36, no. 3, pp. 374–382, Aug. 1989.
[10] K. R. Shouse and D. G. Taylor, "Sensorless velocity control of permanent magnet synchronous motors," *IEEE Trans. Contr. Syst. Technol.*, vol. 6, no. 3, pp. 313–324, May 1998.
[11] L. Harnefors and H. Nee, "A general algorithm for speed and position estimation of AC motors," *IEEE Trans. Ind. Electron.*, vol. 47, no. 1, pp. 77–83, Feb. 2000.
[12] J. Solsona, M. I. Valla, and C. Muravchik, "On speed and rotor position estimation in permanent-magnet AC drives," *IEEE Trans. Ind. Electron.*, vol. 47, no. 5, pp. 1176–1180, Oct. 2000.
[13] T. D. Batzel and K. Y. Lee, "Slotless permanent magnet synchronous motor operation without a high resolution rotor angle sensor," *IEEE Trans. Energy Convers.*, vol. 15, no. 4, pp. 366–371, Dec. 2000.
[14] H. H. Rosenbrock, "The stability of linear time-dependent control systems," *J. Electron. Contr.*, vol. 34, no. 12, pp. 73–80, Jul. 1963.
[15] D. Luenberger, "An introduction to observers," *IEEE Trans. Autom. Control*, vol. AC-16, no. 6, pp. 596–602, Dec. 1971.
[16] W. L. Brogan, *Modern Control Theory*. Upper Saddle River, NJ: Prentice-Hall, 1991.
[17] C. Phillips and R. Harbor, *Feedback Control Systems*, 4th ed. Upper Saddle River, NJ: Prentice Hall, 1999.
[18] R. Krishnan and R. Ghosh, "Starting algorithm and performance of a PM DC brushless motor drive system with no position sensor," in *Proc. Power Electronic Specialists Conf.*, 1986, pp. 815–821.
[19] T. D. Batzel, "Electric propulsion using the permanent magnet synchronous motor without rotor position transducers," Ph.D. thesis, Dept. Elect. Eng., Pennsylvania State Univ., University Park, PA, 2000.
[20] J. Kim and S. Sul, "New approach for high performance PMSM drives without rotational position sensors," *IEEE Trans. Power Electron.*, vol. 12, no. 5, pp. 904–911, Sep. 1997.
[21] Z. Lin, D. Howe, P. Mellor, and M. Jenkins, "Coupled thermal and electromagnetic analysis of a permanent magnet brushless dc servo motor," in *Proc. 6th Int. Conf. Electric Machines Drives*, 1993, pp. 631–635.

**Todd D. Batzel** (M'00) received the B.S. and Ph.D. degrees in electrical engineering from The Pennsylvania State University, University Park, in 1984 and 2000, respectively, and the M.S. degree in electrical engineering from the University of Pittsburgh, Pittsburgh, PA, in 1989.

Currently, he is Assistant Professor of Electrical Engineering at Penn State Altoona. His research interests include electric machines, electric motor controls, power electronics, artificial intelligence applications to control, and embedded control systems.

**Kwang Y. Lee** (F'01) received the B.S. degree in electrical engineering from Seoul National University, Seoul, Korea, in 1964, the M.S. degree in electrical engineering from North Dakota State University, Fargo, in 1968, and the Ph.D. degree in systems science from Michigan State University, East Lansing, in 1971.

Currently, he is a Professor of Electrical Engineering and is Director of Power Systems Control Laboratory at The Pennsylvania State University, University Park. He has also been with Michigan State; Oregon State, Corvallis; and the University of Houston, Houston, TX. His interests include power systems operation and planning, expert systems, and intelligent system applications to power systems.

Dr. Lee is an Associate Editor of IEEE TRANSACTIONS ON NEURAL NETWORKS and an Editor of the IEEE TRANSACTIONS ON ENERGY CONVERSION.